Sun, Z., et al., 2021, Formation of low-gradient bedrock chutes by dry rockfall on planetary surfaces: Geology, https://doi.org/10.1130/G49286.1

Data Repository for

Formation of low-gradient bedrock chutes by dry rockfall on planetary surfaces

Zhongheng Sun[1,2], Thomas P. Ulizio[1], Jade N. Fischer[1], Janette N. Levin[1], Alexander R. Beer[1], James L. Dickson[1], Michael P. Lamb[1*]

[1] Division of Geological and Planetary Sciences, California Institute of Technology, Pasadena, California 91125, USA

[2] Key Laboratory of Tectonics and Petroleum Resources (China University of Geosciences), Ministry of Education, Wuhan 430074, China

[3] Department of Geosciences, University of Tübingen, D-72076 Tübingen, Germany

*mpl@gps.caltech.edu

This PDF file includes:

Data Repository Figures

Figure S1 to S8

Caption for Video S1 to S3

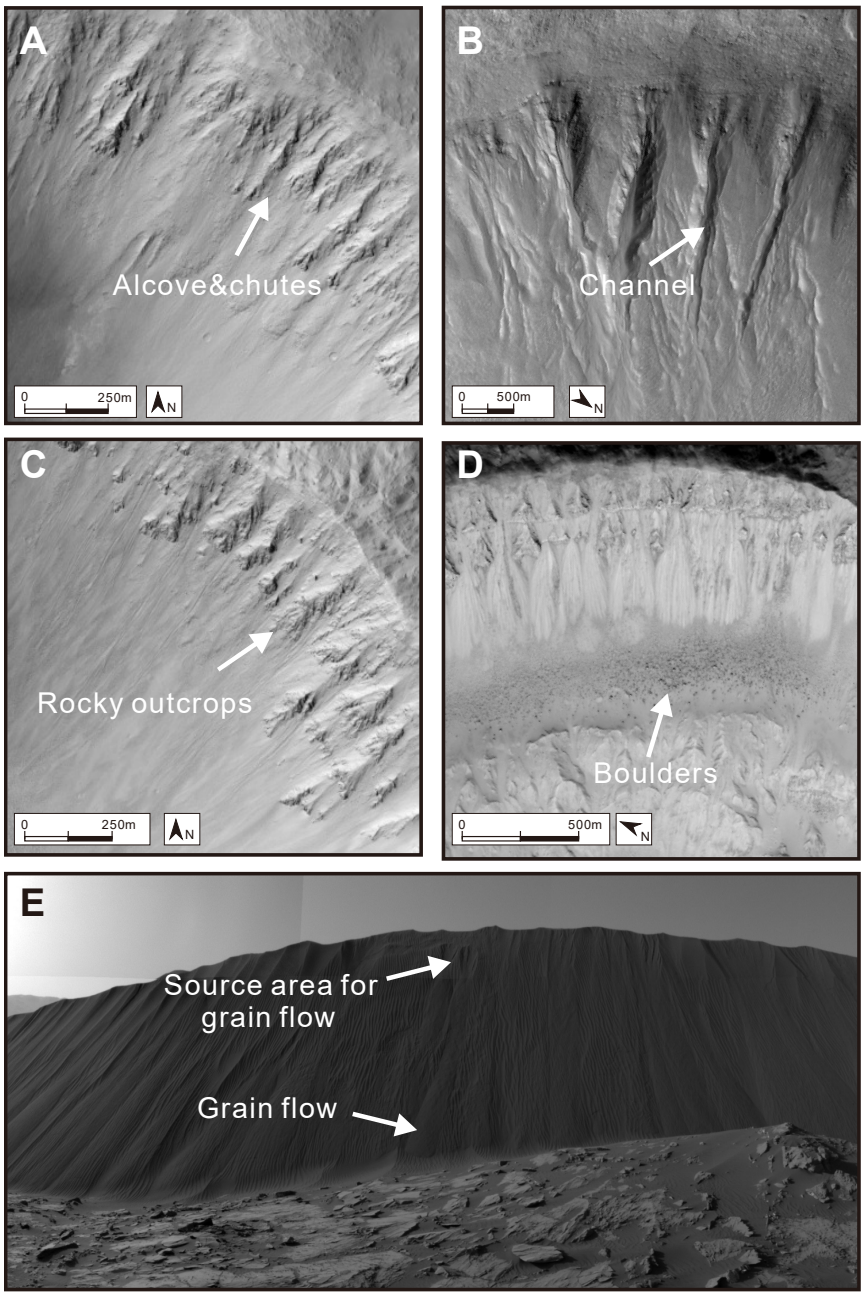

Figure S1. **Martian landforms.** **(A)** HiRISE image ESP_019080_1865 showing bedrock chutes and alcoves. (**B)** HiRISE image ESP_022841_1300 showing gully channels that are potentially in ice-cemented mantling material. (**C)** HiRISE image ESP_035813_1870 showing rocky outcrops on a crater wall. (**D)** HiRISE image ESP_011972_1665 showing large boulders below chutes. (**E**) Grain flow lobes on the 4-m-high slip face of Namib Dune by MSL Curiosity's Navigation Camera. Image credits: NASA/JPL-Caltech/University of Arizona.

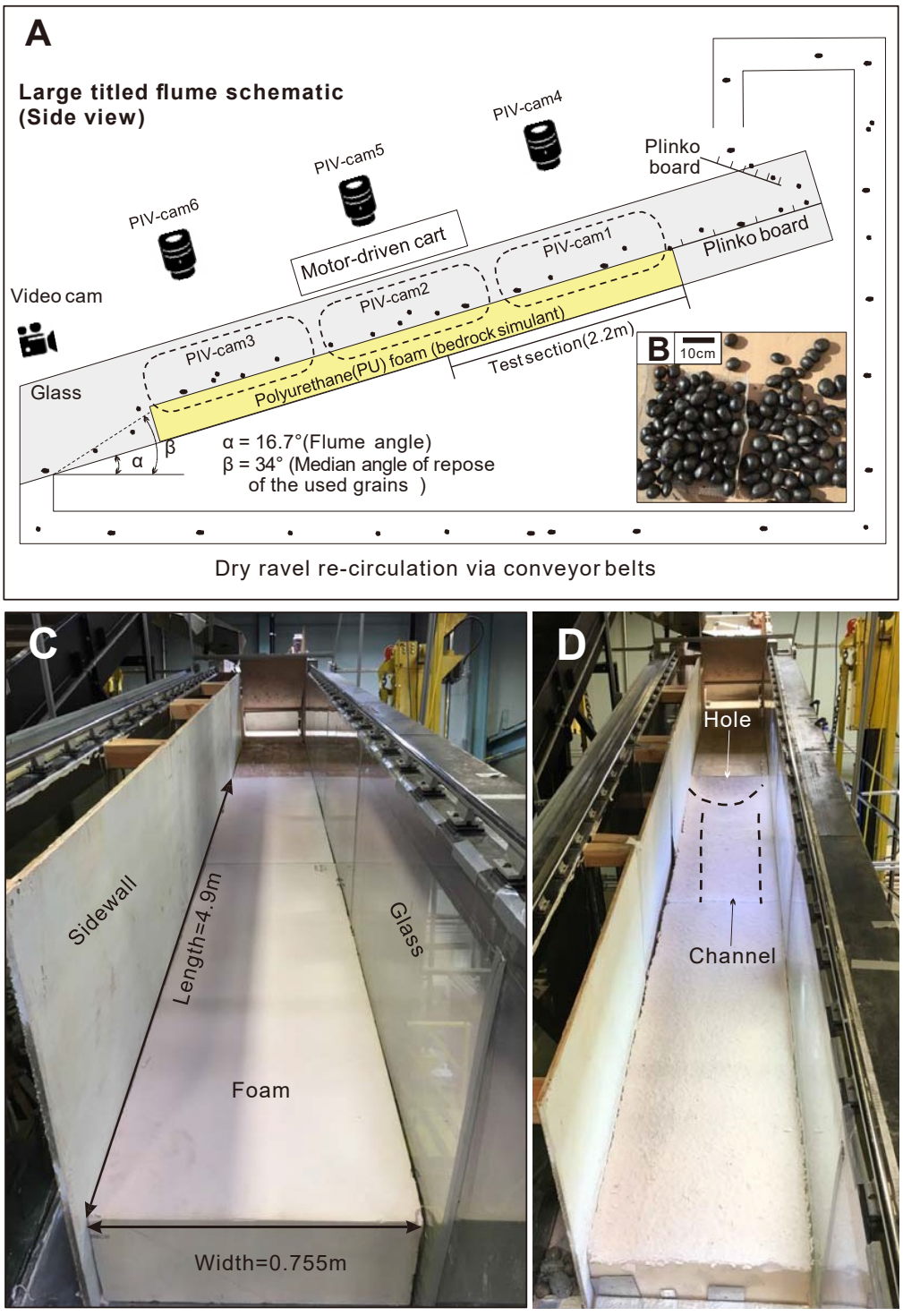

Figure S2. Experimental setup. **(A)** Schematic of the experimental facility. **(B)** Natural grains used in the experiment that were painted black to visualize. **(C)** View looking upslope into the flume at $T^* = 0$. **(D)** View into the flume after completion of the experiment ($T^* = 66{,}400$).

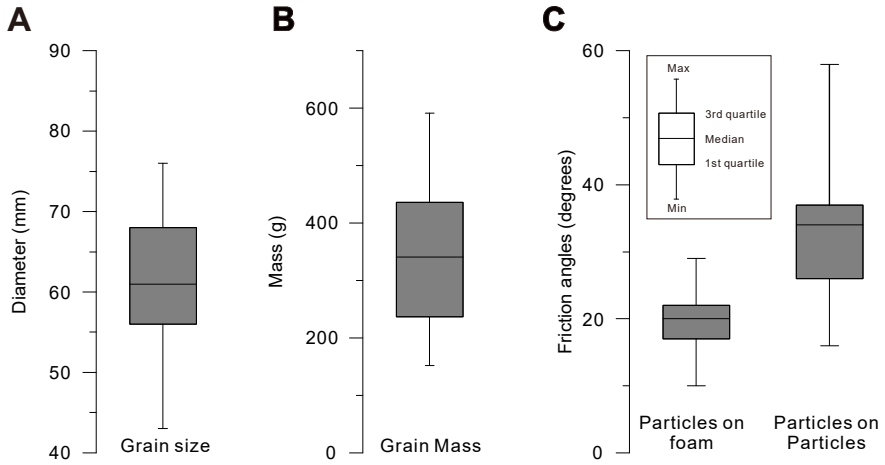

Figure S3. Grain properties. (**A)** Distribution of intermediate particle diameters (Data S1). (**B)** Distribution of particle mass (Data S1). (**C)** Friction angles of particles on the foam bed and on a bed of fixed particles of the same size and shape (Data S2).

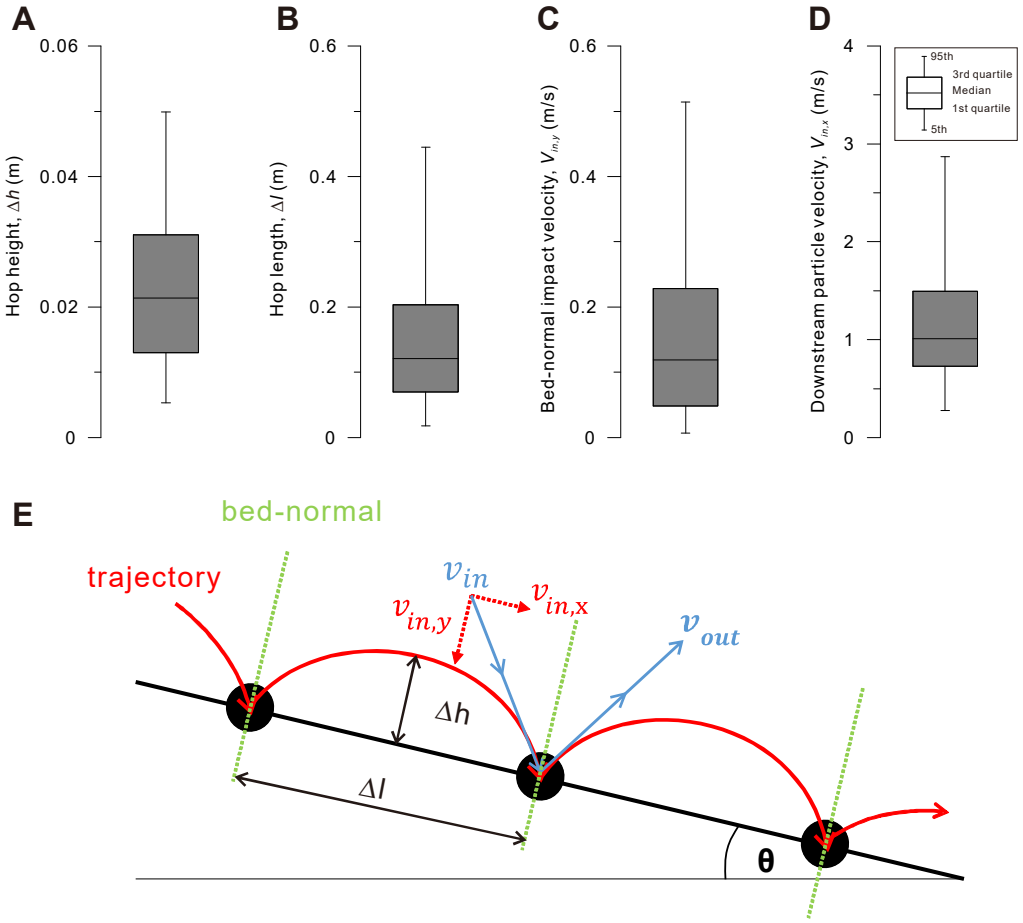

Figure S4. **Grain kinetics** (Data S3). **(A)** Hop heights (Δh), **(B)** hop lengths (Δl), (**C**) bed-normal impact velocities ($v_{in,y}$), and (**D**) downstream particle velocities ($v_{in,x}$). The numbers represent the 202 of grains trajectories measured from time T*=7700 – 66,400. **(E)** Schematic of a particle hopping on a tilted bed.

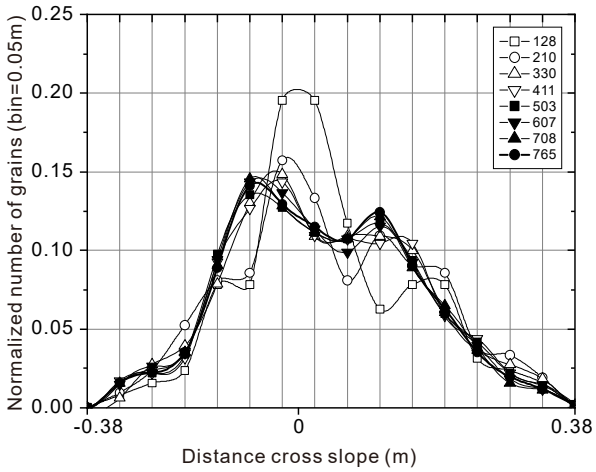

Figure S5. **Cross-slope grain distribution.** Subsampling of cross-slope grain distributions with different number of grains counted, measured at cross-section CS1 (see Fig. 3A) at T^*=66,400, showing that the distributions were consistent when more than 500 grains were counted (Data S5).

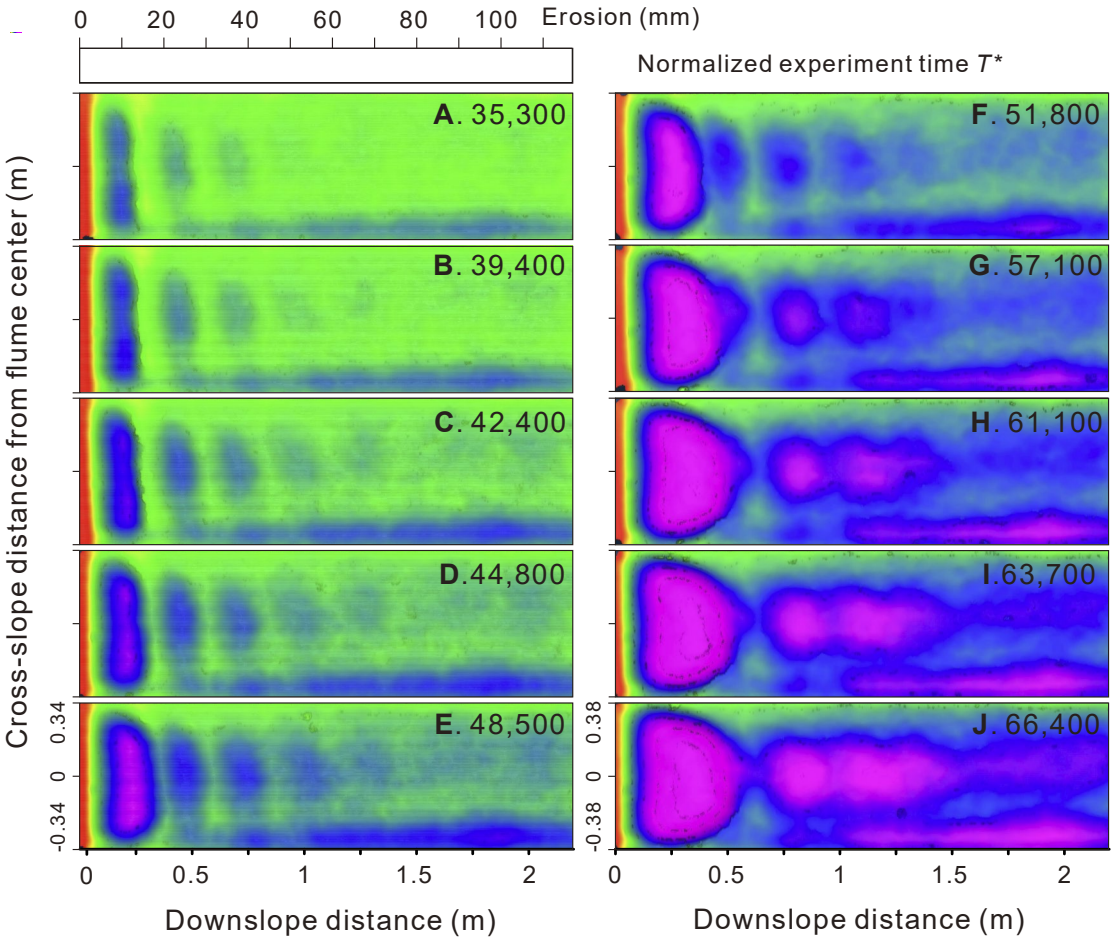

Figure S6. Bedrock topography evolution. Erosion was calculated by subtracting the topography at the noted dimensionless experimental time, T^*, from the initial planar surface elevations.

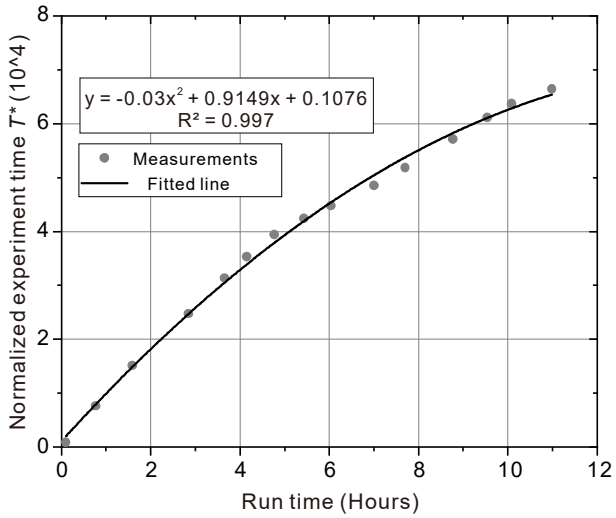

Figure S7. Normalized experiment time T^* as a function of run time (Data S6).

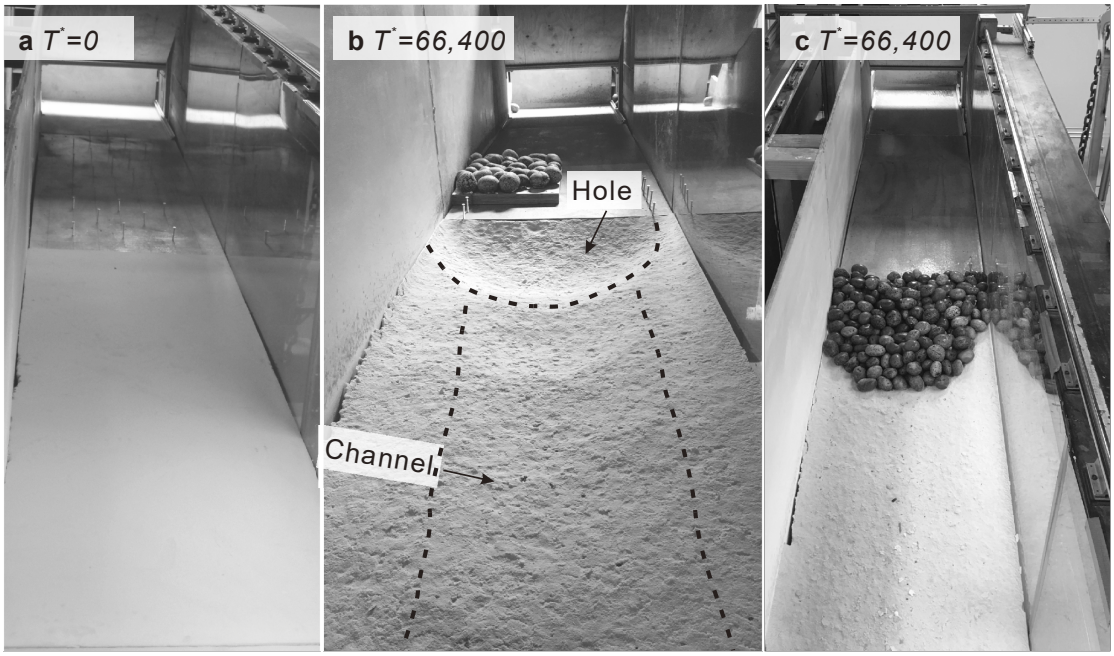

Figure S8. Bedrock comparison before and after the experiment. (**A)** Initial flume bed with planar foam and pegboard upslope. (**B)** Bedrock topography showing formed alcove, trough and gully channel after completion of the experiment (T^*=66,400). (**C)** Same time as panel B but with the upslope hole filled with the static layer of cobbles at the experiment end (T^*=66,400). Note the changed peg board upslope, where most pegs were removed at T^* = 7700.

Videos S1-S3. Oblique overhead video of the experimental test section during active rock fall at T^*=16,900 (Video S1), T^*=36,570 (Video S2) and T^*= 55,500 (Video S3). Note that due to the light color of the foam and lighting used for particle tracking, the topography on the foam is not clearly visualized.